

Red Spiral Galaxies in the Cosmic Noon Unveiled in the First JWST Image

YOSHINOBU FUDAMOTO,^{1,2} AKIO K. INOUE,^{1,3} AND YUMA SUGAHARA^{1,2}

¹Waseda Research Institute for Science and Engineering, Faculty of Science and Engineering, Waseda University, 3-4-1 Okubo, Shinjuku, Tokyo 169-8555, Japan

²National Astronomical Observatory of Japan, 2-21-1, Osawa, Mitaka, Tokyo, Japan

³Department of Physics, School of Advanced Science and Engineering, Faculty of Science and Engineering, Waseda University, 3-4-1, Okubo, Shinjuku, Tokyo 169-8555, Japan

ABSTRACT

In the first image of the James Webb Space Telescope (JWST) of SMACS J0723.3-7327, one of the most outstanding features is the emergence of a large number of red spiral galaxies, because such red spiral galaxies are only a few percent in the number fraction among nearby spiral galaxies. While these apparently red galaxies were already detected with the Spitzer Space Telescope at $\sim 3 - 4\mu\text{m}$, the revolutionized view from JWST's unprecedented spatial resolution has unveiled their hidden spiral morphology for the first time. Within the red spiral galaxies, we focus on the three most highly red galaxies that are very faint in the $< 0.9\mu\text{m}$ bands and show red colors in the $2 - 4\mu\text{m}$ bands. Our study finds that the three extremely red spiral galaxies are likely to be in the Cosmic Noon (i.e., $1 < z < 3$) and could be consistent with passive (i.e., \sim zero star-formation rates) galaxies having moderate dust reddening (i.e., $A_V \sim 1$ mag). These “red spiral” galaxies would be interesting, potentially new population of galaxies, as we start to see their detailed morphology using JWST, for the first time. Finally, we note that the spectral energy distribution of these red $z \sim 2.5$ galaxies could mimic $z > 10$ Lyman break galaxies and contaminate to $z > 10$ galaxy samples, especially when they were faint and small.

Keywords: Spiral galaxies (1560) — Galaxy structure (622) — Galaxy formation (595) — Galaxy evolution (594) — Galaxy stellar disks (1594)

1. INTRODUCTION

The spiral structure of galaxies is not only one of the most spectacular features of the Universe but also provides us with important information of galaxy formation and evolution. Since the first systematic classification of the morphology of “extragalactic nebulae” (Hubble 1926), large efforts have been devoted to studying the morphology of galaxies across cosmic time and to understanding their formation mechanisms (see Conselice 2014, for a review). However, when and how the galaxy morphology emerged in the early Universe is still largely unknown.

Spiral galaxies typically show blue colors in their rest-frame optical wavelength and are, in general, classified as “normal” star-forming galaxies (e.g., Schawinski et al. 2014). Red or passive (i.e. non star-forming or ‘anemic’; van den Bergh 1976) spiral galaxies are, on the other hand, a very minor population in the nearby Universe. In the latest study, Shimakawa et al. (2022) identified nearly a thousand red, passive spiral galaxies among

$\sim 55,000$ galaxies at $0.01 < z < 0.3$ from 1000 deg^2 imaging data obtained with the Subaru/Hyper Suprime-Cam. Hence, the fraction of the red spiral galaxy is only $\sim 2\%$ in the local Universe.

It was, for the first look, surprising to find many apparently red spiral galaxies in the James Webb Space Telescope (JWST) image of the galaxy cluster, SMACS J0723.3-7327, that was released on July 11th 2022 as part of the early release observations (ERO; Pontoppidan et al. 2022). Their redness could indicate several important properties of these spiral galaxies: their dominant stellar ages, dust reddening, or a combination of these features. Because the released image was taken by the Near Infrared Camera (NIRCam) on JWST over the wavelength range of $0.9 - 4.4\mu\text{m}$, the redness in NIR may indicate that these spiral galaxies are at high redshift.

Spiral galaxies in the distant universe are a very important population to examine the emergence of the spiral structure in galaxies. The most distant spiral galaxy known so far is a gas-rich galaxy, BRI 1335-0417,

at $z = 4.41$ (Tsukui & Iguchi 2021). A grand-design spiral structure traced by the [C II] line was revealed with the Atacama Large Millimeter/submillimeter Array (ALMA); however, the stellar structure of BRI 1335-0417 is still unknown. The most distant, spiral stellar disk galaxies are reported at $z = 2$ – 2.5 (Dawson et al. 2003; Law et al. 2012; Margalef-Bentabol et al. 2022). Searching for such galaxies at even higher redshift is the key to knowing when the stellar spiral disks emerged.

To characterize red spiral galaxies found in the JWST’s ERO data, we carefully select the most extreme red spiral galaxies and examine their spectral energy distribution (SED), as a first case study. This Letter is organized as follows: in §2 we describe data and the sample used in this study. In §3, we present our analysis. §4 shows the results and discussion on the red spiral galaxies found in the JWST images. We conclude in §5. Throughout this Letter, we assume a cosmology with $(\Omega_m, \Omega_\Lambda, h) = (0.3, 0.7, 0.7)$

2. DATA

The following images of the Hubble Space Telescope (HST) and JWST are based on a “first-pass” reduction of the HST and JWST images of the SMACS-0723 lensing cluster field. All images have been processed with the *grizli*¹ software pipeline. Further documentation will be provided by G. Brammer et al. (in prep).

2.1. HST data

As part of the Reionization Lensing Cluster Survey: RELICS (Coe et al. 2019), optical and NIR images were obtained using HST. These HST images include data from ACS (F435W, F606W, F814W filters) and WFC3/IR (F105W, F125W, F140W, F160W filters) instruments. All HST data were calibrated and mosaiced in a standard manner. Final images have a pixel scale of $0.04''/\text{pixel}$.

2.2. JWST data

We used JWST NIRCам images of six filters in total (F090W, F150W, F200W, F277W, F356W, and F444W). After the re-processing of the JWST’s public data available in the MAST data archive, the final mosaic has $0.02''/\text{pixel}$ for the short wavelength filters (F090W, F150W, F200W), and $0.04''/\text{pixel}$ for the long wavelength filters (F277W, F356W, F444W). A small astrometric offset exists between HST and JWST images. The offset, however, did not affect our analysis as we manually corrected positions of apertures during our photometry.

¹ <https://github.com/gbrammer/grizli>

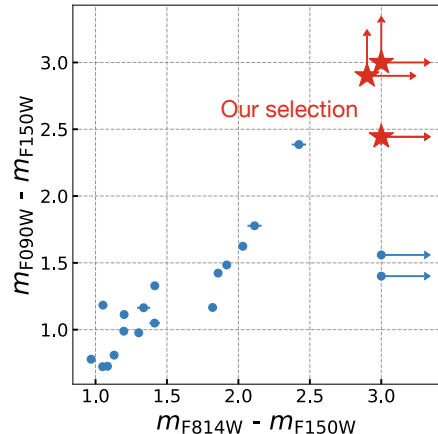


Figure 1. The observed colors of red spiral galaxies. After our visual selections of red spiral galaxies, we further down-selected the most $\sim 1 - 2 \mu\text{m}$ red galaxies, which we focus on in this study (red stars). These galaxies have extremely red colors of $m_{\text{F814W}/\text{F090W}} - m_{\text{F150W}} > 2.5$ mag. Other red spiral galaxies (blue points) have at least one $> 3\sigma$ detection in the HST ACS bands.

3. ANALYSIS

3.1. Selecting Red Spiral Galaxies

We first visually selected bright red spiral galaxies from the false-color image presented within the ERO release². Two authors (Y.F. and A.K.I.) visually selected red spiral galaxies from the image independently. We selected 22 galaxies that both agreed as having spiral structures with apparently red colors. While quantitative evaluation of galaxy types would also be preferred (e.g., Domínguez Sánchez et al. 2018; Ferreira et al. 2022), visual selections are also known to be effective and widely used, especially when finding apparent structures, such as spiral shape (e.g., Galaxy Zoo Project: Lintott et al. 2008).

To find the reddest spiral galaxies, we further down-selected samples based on their faintness in $\leq 0.9 \mu\text{m}$ images (see §3.2.1 below for the photometry of our sample here). In particular, we selected galaxies that are non-detected in the HST F814W image and, at the same time, galaxies that have an extremely red color in the F090W vs. F150W image (Fig. 1).

The selected red spiral galaxies (RS12, RS13, and RS14) were already detected by HST WFC3 and/or Spitzer IRAC images; however, the angular resolution of these previous instruments did not allow us to study detailed morphology. We can now access the resolved morphology of the red spiral galaxies by JWST’s un-

² <https://stsci-opo.org/STScI-01G7DDBW5NNXTJV8PGHB0465QP.png>

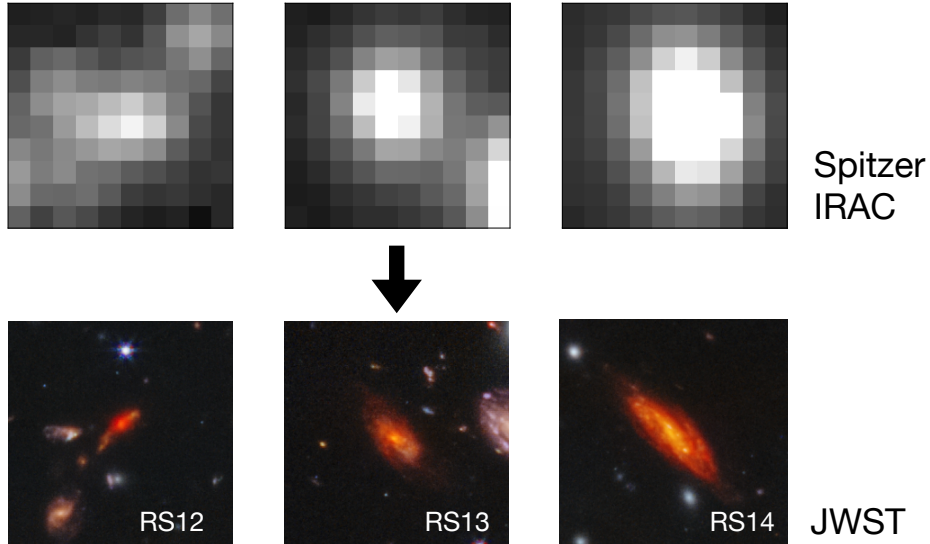


Figure 2. Demonstrations of the improved spatial resolution by JWST observations: (Upper panels) Spitzer IRAC $3.6\ \mu\text{m}$ images of the extremely red spiral galaxies in the SMACS 0723 field. (Lower Panels) False-color images by JWST’s F090W, F150W, F200W, F277W, F356W, and F444W filters. The arm and bulge structure of the galaxies are captured for the first time, thanks to the extremely high resolution and sensitivity of JWST. Position angles have ~ 30 deg offset between Spitzer and JWST images. Copyright: NASA/STScI

precedented spatial resolution and sensitivity in these NIR wavelengths (Fig. 2).

3.2. Photometry

3.2.1. HST and JWST photometry

To measure galaxy-wide integrated fluxes, we performed aperture photometry of both HST and JWST images for the red spiral galaxies. We used python package `photutils` (Bradley et al. 2020) using elliptical apertures. We applied apertures large enough to enclose entire galaxies in the JWST F444W image to obtain integrated fluxes. Measured flux errors incorporated background noises by scaling pixel-by-pixel root mean squares (RMSs) to aperture sizes, and Poisson noises of measured fluxes.

We corrected the photometric zero-point of JWST images based on the first commissioning report (Table 4 of Rigby et al. 2022). The correction was not significant for the three short wavelength filters but up to $\sim 20\%$ for the three long wavelength filters. These updated zero-points were, however, based on preliminary calibrations of JWST. Therefore, further uncertainties could still be expected. To incorporate such uncertainties, we additionally applied 10% of flux uncertainties for all measured fluxes from JWST. These uncertainties were added quadratically to the measured aperture flux errors.

3.2.2. RS14

Within the extremely red spiral galaxies, RS14 has already been studied in several papers. In particular, Sun et al. (2022) reported ALMA continuum detection in 1.1 mm image obtained among the ALMA large program ALCS: 2018.1.00035.L (PI: K. Kohno). Most recently, Cheng et al. (2022) presented a joint JWST-ALMA study of this source. Also, Carnall et al. (2022) reported spectroscopic redshift of $z_{\text{spec}} = 2.463$ determined by multiple emission lines such as $\text{H}\alpha$, [NII], and [SII] emission lines (ID 9239 of NIRSpec spectroscopy as part of the same JWST ERO). In the following analysis, we used the ALMA continuum flux and the NIRSpec redshift for RS14.

3.3. Lensing Magnification

We estimated gravitational lensing magnification based on the recent work by Golubchik et al. (2022). Their lens model is constructed with `Light-Traces-Mass` method (e.g., Broadhurst et al. 2005), which infers the lens mass contributions from the cluster’s light distributions, using HST and VLT MUSE data. We estimated lensing magnification factors by assuming redshifts from the following SED fittings.

3.4. Spectral Energy Distribution fittings

To constrain the physical properties and redshift of our extremely red spiral galaxies, we used SED fitting code `PANHIT` (Mawatari et al. 2020). We assumed a Chabrier initial mass function in a range of 0.1–100 M_{\odot} (Chabrier 2003), the BC03 stellar population model

(Bruzual & Charlot 2003), a nebular continuum and line emission model (Inoue 2011), and a standard dust attenuation curve (Calzetti et al. 2000). The star formation history was assumed to be the “delayed- τ ” model (Speagle et al. 2014) to describe a variety of star formation histories, and the star-formation time-scale τ_{SF} is a free parameter between 0.01 and 10 Gyr. We allowed for metallicities ranging from $0.005 \times Z_{\odot}$ to $2.5 \times Z_{\odot}$, where the Solar metallicity of $Z_{\odot} = 0.02$. The dust attenuation in the V -band (A_V) is also a free parameter. The age of the stellar population is another free parameter between 1 Myr and 15 Gyr, and the cosmic age limits it at the redshift of interest. The redshift is the final free parameter and we examined redshifts from 0.1 to 13.0 with a step of 0.1. The stellar mass and star formation rate (SFR) were determined by scaling the amplitude of the SED. The SED fits performed χ^2 minimization algorithm for the photometry data, including non-detection bands (i.e., upper limits; Sawicki 2012).

For RS14, we run the fitting with the spectroscopic redshift of $z = 2.463$ (Carnall et al. 2022) and including the ALMA continuum flux (Cheng et al. 2022). PANHIT assumes energy conservation between the stellar radiation absorbed by dust and the far-infrared (FIR) emission from dust. We assumed modified black-body functions with an emissivity index $\beta = 2$ and the dust temperature, T_d , between 10 and 50 K with a step of 5 K. Note that the cosmic microwave background temperature at $z = 2.463$ is 9.5 K, a strict lower limit of T_d .

4. RESULTS AND DISCUSSION

4.1. SED fitting results

We found that the photometric redshifts of extremely red spirals are likely to be in a range of $z_{\text{ph}} = 1\text{--}3$ for RS12 and RS13. The spectroscopic redshift of $z_{\text{sp}} = 2.463$ of RS14 is also in the redshift range. In particular, RS14 ($z_{\text{spec}} = 2.463$) is one of the highest redshift spiral galaxies identified so far (Dawson et al. 2003; Law et al. 2012; Margalef-Bentabol et al. 2022).

Furthermore, the integrated properties of the extremely red spiral galaxies at $1 < z < 3$ seems to be dominated by old stellar population, and are consistent with almost completely passive, non star-forming galaxies. In our SED fits, these passiveness are indicated from the JWST’s coverage of $\lambda_{\text{rest}} \sim 4300\text{--}12800 \text{ \AA}$ photometry, and the red colors of these bands can be explained by old stellar populations with moderate dust attenuation. It is surprising to find large amount of red and dead spiral galaxies, as they are very rare in the local Universe (Shimakawa et al. 2022).

We note that our SED fit results would have some caveats, such as uncertain calibration of JWST pho-

tometry, which would change observed colors of these galaxies (see also Morishita & Stiavelli 2022, for different photometric zero-point corrections). Also, the physical properties of these red spiral galaxies are not well studied yet. Thus, other assumptions, that are not included in our SED fits, could be allowed; such as steeper dust attenuation curve or recent busy star-formation activity completely obscured by dust. Thus, we caution readers that this study report one of the possible interpretations of these interesting red spiral galaxies at high-redshift, newly revealed by JWST. We encourage further analysis to investigate more details of these exciting galaxies.

Table 1 is a summary of the fitting results as well as the lensing magnification factors. Following, we describe results of our SED fitting in detail:

4.1.1. RS12

RS12 was initially identified in Sun et al. (2021, ID: ES-025) through an extensive survey of NIR-dark galaxies in lensing cluster fields, which could be at $z \simeq 3\text{--}5$ through their stacking analysis. In our SED fits (top panel of Fig. 3), we found a global χ^2 minimum in a range of $1 \lesssim z \lesssim 3$ (right panel).

The most likely redshift solution is $z_{\text{ph}} = 2.5 \pm 0.3$. For this solution, we found that RS12 is a passive galaxy with an age of about 1 Gyr. Since the age is much longer than the star-formation time-scale, $\tau_{\text{SF}} \lesssim 0.1$ Gyr, the current SFR_e is almost zero. The stellar mass is about $2 \times 10^{10} M_{\odot}$ after correcting for a lensing magnification of $\mu = 1.68$ at $z_{\text{ph}} = 2.5$. The stellar mass is in the lower end of high- z passive galaxies known so far (Marchesini 2022). The dust attenuation is somewhat large as $A_V \sim 1.7$. Metallicity of the stellar population was not constrained much.

Another sharp χ^2 minimum was found at $z_{\text{ph}} = 2.1$. This solution represents an extremely young, dusty starburst line emitter. In this model, the majority of fluxes seen in NIRC_{am} bands are produced by strong optical-to-NIR nebular lines, instead of the stellar continuum (see the gray curve in the top panel of Fig. 3). The SFR is abnormally high as $\sim 10^4 M_{\odot} \text{ yr}^{-1}$ and the age is extremely young as ~ 1 Myr. The dust attenuation is also very high as $A_V \sim 6$ mag. Given a small probability to observe such a short time-scale system as well as the abnormal properties, this solution is merely theoretical and very unlikely.

Yet another interesting redshift solution was found at $z = 10.8 \pm 0.2$. This is a very high- z Lyman break galaxy (LBG) solution. The non-detections below the $1 \mu\text{m}$ bands are explained by the Ly α break. Due to the brightness of the source (24 AB in F200W, ~ 22.5 AB mag at $\sim 4.4 \mu\text{m}$; this work and Sun et al.

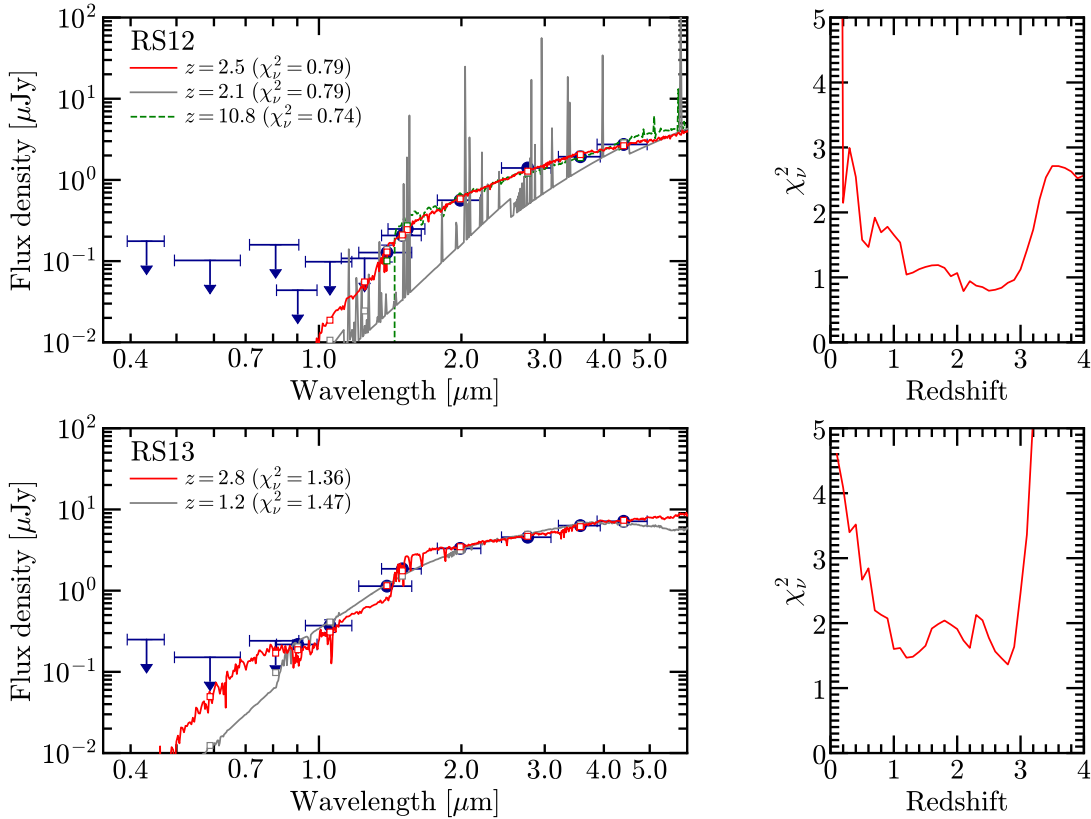


Figure 3. SED fitting results of RS12 (upper panels) and RS13 (lower panels): For both galaxies, left panels show the SEDs inferred from our fitting. Right panels show reduced χ^2_ν as a function of redshift. For RS12, three different redshift solutions are almost equally possible, including an extremely high-redshift one at $z = 10.8$. However, the solutions of $z = 10.8$ and $z = 2.1$ are unlikely (see discussions in § 1). For RS13, photometric redshift is also loosely constrained at $1 < z < 3$. For both galaxies, passive solutions at $1 < z < 3$ (with $\text{SFR} \sim 0$ to $\sim 1/\mu M_\odot \text{yr}^{-1}$) are the best-fit (red solid lines in left panels).

2021, respectively)), however, the SFR and the stellar mass, in this high- z solution, are abnormally large as $\sim 3 \times 10^3 M_\odot \text{yr}^{-1}$ and $\sim 1 \times 10^{11} M_\odot$ after correcting a lensing magnification of $\mu = 1.88$. The red continuum slope requires a large dust attenuation of $A_V \sim 2$ mag. Although this massive “red” LBG solution is very interesting, it is also unlikely due to its predicted abnormally high integrated SFR.

4.1.2. RS13

Similarly, we found a global χ^2 minimum in the redshift range of $1 \lesssim z \lesssim 3$ (lower right panel of Fig. 3), showing two local minima at $z = 1.2$ and $z = 2.8$.

The best redshift solution of RS13 is $z_{\text{ph}} = 2.8 \pm 0.1$. For this solution, RS13 is a passive galaxy (SFR consistent with zero) with the stellar age of 0.4 Gyr, showing the clear Balmer break around F140W and F150W filter wavelengths. The stellar mass is $\sim 2 \times 10^{10} M_\odot$ after correcting a magnification. Metallicity of the stellar population is higher than half of the solar value.

Another redshift solution is $z_{\text{ph}} = 1.2 \pm 0.2$, having a large dust reddening of $A_V = 3.5^{+0.4}_{-1.3}$ with SFR almost consistent with zero. This solution explains non-

detections below $0.8 \mu\text{m}$ with the Balmer break and red colors at longer wavelengths with a dusty stellar continuum. The stellar metallicity, in this case, is only loosely constrained but is suggested to be very low $Z < 0.04 Z_\odot$. Given the assumed low metallicity in spite of the large dust attenuation, the $z_{\text{ph}} = 1.2$ solution is less likely.

4.1.3. RS14

We found that the $T_d = 15$ K case delivered the minimum χ^2 value compared to other T_d cases. Higher T_d with fixing 1.1 mm flux leads to larger IR luminosity, and thus, larger dust attenuation; however, it makes the rest-frame optical SED traced by NIRCcam too red. As such, the $T_d = 15$ K, rather low temperature (e.g., Schreiber et al. 2018), seems the best representation for RS14, that is shown in Fig. 4.

The best-fit model for RS14 is again passive, old stellar population, and moderate dust attenuation ($A_V = 0.84^{+0.16}_{-0.06}$). Similar to RS12, the age is much longer than the star-formation time-scale, $\tau_{\text{SF}} \lesssim 0.1$ Gyr, and the current SFR is almost zero. This feature support the very low T_d (15 K) that is heated by old stars rather than massive young stars. The stellar mass is relatively

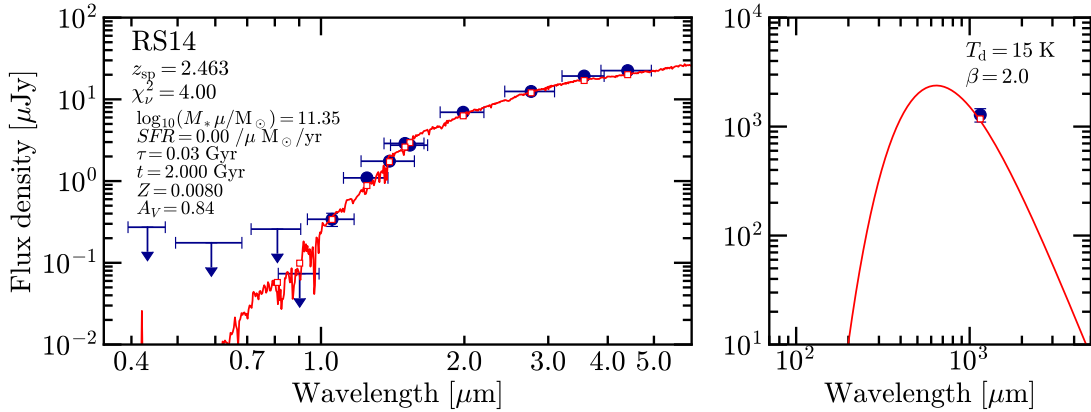


Figure 4. The best fit SED of RS14 derived by fixing its redshift at $z_{\text{sp}} = 2.463$. The JWST’s photometry can be represented solely by old stellar populations, thus not requiring considerable dust reddening and star formation. The SED fitting results indicate that RS14 represents a passive spiral galaxy at high redshift.

high, $1.0 \times 10^{11} M_{\odot}$ after correcting a magnification of $\mu = 2.16$ at $z_{\text{spec}} = 2.463$.

While the galaxy-wide integrated property of RS14 is consistent with non-star-forming passive galaxy, JWST’s F090W image (the rest-frame wavelength of $\sim 2600 \text{ \AA}$) shows a few faint clumps in the bulge and some parts of the spiral arm region of RS14, which is not smoothed out by our photometry using a large aperture. As these clumps can be seen in the rest-frame UV wavelength, a small amount of star-formation activity is still on-going in RS14. This is also consistent with the $\text{H}\alpha$ emission line detection (Carnall et al. 2022). Also, if there is completely dust-obscured activity in RS14, the rest-frame optical SED shape (i.e. tracer of dust attenuation) and the 1.1 mm dust continuum flux can be decoupled, and our assumption of the radiation energy balance in the SED analysis would break down. Hence, RS14 may have a substantial star-formation.

4.2. Lyman break or Balmer break?

As we have seen in RS12, some of the red $z \sim 2$ galaxies can mimic $z \gtrsim 10$ star-forming galaxies because of the famous confusion between Lyman break and Balmer break (or 4000 \AA break for passive galaxies). Especially, high-redshift ($z > 7$) galaxies sometimes have extremely red colors in their rest-frame UV continuum (e.g., UV continuum slope $\beta > -1.5$; Roberts-Borsani et al. 2022), making it further difficult to discern between Lyman and Balmer breaks. Spectroscopy would, thus, serve as an essential step to study such cases.

5. CONCLUSION

In this paper, we studied the properties of three extremely red spiral galaxies (RS12, RS13, and RS14) found from the JWST ERO image data release of SMACS 0723. These extremely red spiral galaxies are among a sample of red spiral galaxies visually selected

from the ERO data. By performing SED fitting to the extremely red spiral galaxies, we found the following results:

- Most likely redshifts of the extremely red spirals are $1 < z < 3$, i.e., in the Cosmic Noon. The results show that these red spiral galaxies in JWST images contain the most distant spiral galaxies known to date. Within them, RS14 is currently one of the most distant stellar-spiral galaxy, having $z_{\text{spec}} = 2.463$.
- Surprisingly, our SED fits suggest that the extremely red spiral galaxies are passive galaxies, dominated by old stellar populations. The JWST’s photometry indicates the passiveness from the red colors of the rest-frame wavelength of $\sim 4300 - 12800 \text{ \AA}$. The spectral shape of these bands can be explained by old stellar populations with moderate dust attenuation. This result shows us the possibly counter intuitive picture; we found an extremely old galaxy in the youngest universe explored by the spiral galaxy population, while locally, these spirals are expected to be young star-forming galaxies.
- In some cases, these extremely red sources can mimic $z > 7$ galaxies that have red rest-frame UV colors. We successfully discerned such cases based on the brightness or size of galaxies. However, it would be more challenging if these galaxies were faint or small.

Further detailed studies would be required to understand the formation mechanisms and evolutionary path of the red spiral galaxies. Follow-up observations using integral field spectroscopy, including high-resolution ALMA observations, will provide kinematics, molecular gas, and dust structure of high-redshift spiral galaxies.

Table 1. A summary of SED fitting results and lensing magnification factors.

	RS12	best fit		
z_{ph}		2.5 ± 0.3	2.1	10.8 ± 0.2
χ^2_ν		0.79	0.79	0.74
$\log_{10}(M_* \times \mu [M_\odot])$		$10.50^{+0.37}_{-0.05}$	~ 9.7	$11.39^{+0.14}_{-0.12}$
$SFR \times \mu (M_\odot \text{ yr}^{-1})$		$0.00^{+0.61}$	$\sim 1 \times 10^4$	$4.7^{+3.9}_{-1.1} \times 10^3$
A_V (mag)		$1.7^{+1.3}_{-0.6}$	~ 5.9	2.0 ± 0.2
Age (Gyr)		$1.0^{+1.0}_{-0.6}$	~ 0.001	$0.03^{+0.11}_{-0.01}$
τ_{SF} (Gyr)		0.01–0.14	~ 0.6	0.01–10
Z		0.0001–0.04	0.0001–0.04	0.03–0.05
μ		1.68 ± 0.02	1.64 ± 0.02	$1.88^{+0.04}_{-0.02}$
RS13				
z_{ph}		2.8 ± 0.1	1.2 ± 0.2	
χ^2_ν		1.36	1.47	
$\log_{10}(M_* \times \mu [M_\odot])$		$10.67^{+0.09}_{-0.06}$	10.45 ± 0.22	
$SFR \times \mu (M_\odot \text{ yr}^{-1})$		$0.04^{+0.99}_{-0.04}$	$1.1^{+19.2}_{-1.1}$	
A_V (mag)		$0.5^{+0.5}_{-0.2}$	$3.5^{+0.4}_{-1.3}$	
Age (Gyr)		$0.4^{+0.2}_{-0.1}$	$0.8^{+2.5}_{-0.6}$	
τ_{SF} (Gyr)		0.01–0.06	0.01–2.3	
Z		0.01–0.05	0.0001–0.0008	
μ		1.75 ± 0.03	1.44 ± 0.02	
RS14				
z_{sp}		2.463		
χ^2_ν		4.00		
$\log_{10}(M_* \times \mu [M_\odot])$		$11.35^{+0.09}_{-0.02}$		
$SFR \times \mu (M_\odot \text{ yr}^{-1})$		0.00		
A_V (mag)		$0.84^{+0.16}_{-0.06}$		
Age (Gyr)		$2.0^{+0.0}_{-0.1}$		
τ_{SF} (Gyr)		0.02–0.1		
Z		0.007–0.022		
T_{dust} (K)		~ 15		
μ		2.16 ± 0.06		

We thank Fengwu Sun, Ryosuke Uematsu, and Marc Postman for very helpful discussions. Y.F., A.K.I., and Y.S. acknowledge support from NAOJ ALMA Scientific Research Grant number 2020-16B. The Early Release Observations and associated materials were developed, executed, and compiled by the ERO production team: Hannah Braun, Claire Blome, Matthew Brown, Margaret Carruthers, Dan Coe, Joseph DePasquale, Nestor Espinoza, Macarena Garcia Marin, Karl Gordon, Alaina Henry, Leah Hustak, Andi James, Ann Jenkins, Anton Koekemoer, Stephanie LaMassa, David Law, Alexandra Lockwood, Amaya Moro-Martin, Susan Mullally, Alyssa Pagan, Dani Player, Klaus Pontoppidan, Charles Proffitt, Christine Pulliam, Leah Ramsay, Swara Ravindranath, Neill Reid, Massimo Robberto, Elena Sabbi, Leonardo Ubeda. The EROs were also made possible by the foundational efforts and support from the JWST instruments, STScI planning and scheduling, and Data Management teams.

Facilities: HST, JWST (STIS)

Software: astropy (Astropy Collaboration et al. 2013, 2018), photutils (Bradley et al. 2020), PANHIT (Mawatari et al. 2020)

REFERENCES

- Astropy Collaboration, Robitaille, T. P., Tollerud, E. J., et al. 2013, *A&A*, 558, A33, doi: [10.1051/0004-6361/201322068](https://doi.org/10.1051/0004-6361/201322068)
- Astropy Collaboration, Price-Whelan, A. M., Sipőcz, B. M., et al. 2018, *AJ*, 156, 123, doi: [10.3847/1538-3881/aabc4f](https://doi.org/10.3847/1538-3881/aabc4f)
- Bradley, L., Sipőcz, B., Robitaille, T., et al. 2020, *astropy/photutils*: 1.0.0, 1.0.0, Zenodo, doi: [10.5281/zenodo.4044744](https://doi.org/10.5281/zenodo.4044744)
- Broadhurst, T., Benítez, N., Coe, D., et al. 2005, *ApJ*, 621, 53, doi: [10.1086/426494](https://doi.org/10.1086/426494)
- Bruzual, G., & Charlot, S. 2003, *MNRAS*, 344, 1000, doi: [10.1046/j.1365-8711.2003.06897.x](https://doi.org/10.1046/j.1365-8711.2003.06897.x)
- Calzetti, D., Armus, L., Bohlin, R. C., et al. 2000, *ApJ*, 533, 682, doi: [10.1086/308692](https://doi.org/10.1086/308692)
- Carnall, A. C., Begley, R., McLeod, D. J., et al. 2022, arXiv e-prints, arXiv:2207.08778, <https://arxiv.org/abs/2207.08778>
- Chabrier, G. 2003, *PASP*, 115, 763, doi: [10.1086/376392](https://doi.org/10.1086/376392)
- Cheng, C., Yan, H., Huang, J.-S., et al. 2022, arXiv e-prints, arXiv:2207.08234, <https://arxiv.org/abs/2207.08234>
- Coe, D., Salmon, B., Bradač, M., et al. 2019, *ApJ*, 884, 85, doi: [10.3847/1538-4357/ab412b](https://doi.org/10.3847/1538-4357/ab412b)
- Conselice, C. J. 2014, *ARA&A*, 52, 291, doi: [10.1146/annurev-astro-081913-040037](https://doi.org/10.1146/annurev-astro-081913-040037)
- Dawson, S., McCrady, N., Stern, D., et al. 2003, *AJ*, 125, 1236, doi: [10.1086/367792](https://doi.org/10.1086/367792)
- Domínguez Sánchez, H., Huertas-Company, M., Bernardi, M., Tuccillo, D., & Fischer, J. L. 2018, *MNRAS*, 476, 3661, doi: [10.1093/mnras/sty338](https://doi.org/10.1093/mnras/sty338)
- Ferreira, L., Adams, N., Conselice, C. J., et al. 2022, arXiv e-prints, arXiv:2207.09428, <https://arxiv.org/abs/2207.09428>
- Golubchik, M., Furtak, L. J., Meena, A. K., & Zitrin, A. 2022, arXiv e-prints, arXiv:2207.05007, <https://arxiv.org/abs/2207.05007>
- Hubble, E. P. 1926, *ApJ*, 64, 321, doi: [10.1086/143018](https://doi.org/10.1086/143018)
- Inoue, A. K. 2011, *MNRAS*, 415, 2920, doi: [10.1111/j.1365-2966.2011.18906.x](https://doi.org/10.1111/j.1365-2966.2011.18906.x)
- Law, D. R., Shapley, A. E., Steidel, C. C., et al. 2012, *Nature*, 487, 338, doi: [10.1038/nature11256](https://doi.org/10.1038/nature11256)
- Lintott, C. J., Schawinski, K., Slosar, A., et al. 2008, *MNRAS*, 389, 1179, doi: [10.1111/j.1365-2966.2008.13689.x](https://doi.org/10.1111/j.1365-2966.2008.13689.x)
- Marchesini, D. 2022, arXiv e-prints, arXiv:2207.13625, <https://arxiv.org/abs/2207.13625>
- Margalef-Bentabol, B., Conselice, C. J., Haeussler, B., et al. 2022, *MNRAS*, 511, 1502, doi: [10.1093/mnras/stac080](https://doi.org/10.1093/mnras/stac080)
- Mawatari, K., Inoue, A. K., Yamanaka, S., Hashimoto, T., & Tamura, Y. 2020, in *Panchromatic Modelling with Next Generation Facilities*, ed. M. Boquien, E. Lusso, C. Gruppioni, & P. Tissera, Vol. 341, 285–286, doi: [10.1017/S1743921319002606](https://doi.org/10.1017/S1743921319002606)
- Morishita, T., & Stiavelli, M. 2022, arXiv e-prints, arXiv:2207.11671, <https://arxiv.org/abs/2207.11671>

- Pontoppidan, K., Blome, C., Braun, H., et al. 2022, arXiv e-prints, arXiv:2207.13067.
<https://arxiv.org/abs/2207.13067>
- Rigby, J., Perrin, M., McElwain, M., et al. 2022, arXiv e-prints, arXiv:2207.05632.
<https://arxiv.org/abs/2207.05632>
- Roberts-Borsani, G., Morishita, T., Treu, T., et al. 2022, arXiv e-prints, arXiv:2207.11387.
<https://arxiv.org/abs/2207.11387>
- Sawicki, M. 2012, PASP, 124, 1208, doi: [10.1086/668636](https://doi.org/10.1086/668636)
- Schawinski, K., Urry, C. M., Simmons, B. D., et al. 2014, MNRAS, 440, 889, doi: [10.1093/mnras/stu327](https://doi.org/10.1093/mnras/stu327)
- Schreiber, C., Elbaz, D., Pannella, M., et al. 2018, A&A, 609, A30, doi: [10.1051/0004-6361/201731506](https://doi.org/10.1051/0004-6361/201731506)
- Shimakawa, R., Tanaka, M., Bottrell, C., et al. 2022, PASJ, 74, 612, doi: [10.1093/pasj/psac023](https://doi.org/10.1093/pasj/psac023)
- Speagle, J. S., Steinhardt, C. L., Capak, P. L., & Silverman, J. D. 2014, ApJS, 214, 15, doi: [10.1088/0067-0049/214/2/15](https://doi.org/10.1088/0067-0049/214/2/15)
- Sun, F., Egami, E., Pérez-González, P. G., et al. 2021, ApJ, 922, 114, doi: [10.3847/1538-4357/ac2578](https://doi.org/10.3847/1538-4357/ac2578)
- Sun, F., Egami, E., Fujimoto, S., et al. 2022, ApJ, 932, 77, doi: [10.3847/1538-4357/ac6e3f](https://doi.org/10.3847/1538-4357/ac6e3f)
- Tsukui, T., & Iguchi, S. 2021, Science, 372, 1201, doi: [10.1126/science.abe9680](https://doi.org/10.1126/science.abe9680)
- van den Bergh, S. 1976, ApJ, 206, 883, doi: [10.1086/154452](https://doi.org/10.1086/154452)